ISSN 1990-7931, Russian Journal of Physical Chemistry B, 2022, Vol. 16, No. 1, pp. 1–8. © Pleiades Publishing, Ltd., 2022.
Russian Text © The Author(s), 2022, published in Khimicheskaya Fizika, 2022, Vol. 41, No. 2, pp. 3–11.

STRUCTURE OF CHEMICAL COMPOUNDS, QUANTUM CHEMISTRY, SPECTROSCOPY

Molecular Docking of Cyanine and Squarylium Dyes with NSP15 Endoribonuclease of the SARS-CoV-2 Coronavirus

P. G. Pronkin[a], * and A.S. Tatikolov[a]

[a] *Emanuel Institute of Biochemical Physics, Russian Academy of Sciences, Moscow, Russia*

**e-mail: pronkinp@gmail.com*

Received July 27, 2021; revised August 16, 2021; accepted August 20, 2021

Abstract—The ongoing spread of the COVID-19 coronavirus infection requires us to find new tools and methods for detecting and studying the infection and preventing morbidity (new analytical procedures and tests). With the aim of developing probes for the detection of SARS-CoV-2 coronavirus by modeling *in silico* (molecular docking), the noncovalent binding of cyanine and squarylium dyes with different molecular charges and different types of heterocyclic residues and substituents (42 compounds in total) with different variants of the NSP15 endoribonuclease of the SARS-CoV-2 coronavirus (COVID-19) of the original (wild) type and mutant types is studied. The interaction energies and spatial configurations of the dye molecules in complexes with NSP15 are determined. Some dyes with negative values of the total energy of the complex E_{tot} are promising for further practical study as probes for coronavirus.

Keywords: SARS-CoV-2 coronavirus (COVID-19), NSP15 endoribonuclease, cyanine dyes, squarylium dyes, noncovalent interactions, molecular docking

DOI: 10.1134/S1990793122010262

INTRODUCTION

The threat of the ongoing spread of the SARS-CoV-2 (COVID-19) coronavirus, which is accompanied by its mutations, requires us to develop new procedures and tests to detect, study, and prevent the spread of the virus. One of the most effective approaches currently used in viral research involves the use of fluorescent probes and labels such as cyanine dyes [1–4] (in particular, oxamonomethinecyanines [5]). The main advantages of cyanine dyes are their high extinction coefficients, absorption and emission in the spectral range from UV to IR, overlapping the optical transparency window of biological samples, as well as their unique photophysical and photochemical properties, depending on the molecular environment [6]. The noncovalent interaction of cyanine dyes with biomolecules (nucleic acids, proteins) leads to a change in the photophysical and photochemical properties of the dyes and often proceeds with a multiple increase in fluorescence, which creates preconditions for the use of cyanines as probes in natural and artificial systems containing biomacromolecules [7–12]. The variety of structures and properties of different types of cyanine dyes (which contain polymethine chains of different lengths, as well as different terminal heterocycles and substituents) requires molecular modeling in silico for the preliminary screening of the compounds [13–15]. We have previously studied the interaction between various polymethine (cyanine) dyes (45 compounds in total) and the spike protein (S) SARS-CoV-2 in silico (by molecular docking) [16]. In this study, using the modeling method in silico (molecular docking), the study of the interaction of cyanine dyes with the molecular components of the SARS-CoV-2 coronavirus was continued: the interaction of various types of dyes (42 compounds) with different types of the enzyme protein of the SARS-CoV-2 virus, NSP15 endoribonuclease, was simulated: as the original (wild) type and mutant types.

EXPERIMENTAL

Molecular docking was performed using the DockThor site [17–19]. In the experiment, we used the target protein structures proposed on the DockThor website; as a reference, we studied the wild type of protein-enzyme NSP15 (PDB-code: 6wxc), corresponding to the reference sequence of the virus' genome (isolated in Wuhan, Hubei province, China, December 2019) [20]. Docking was also performed with four mutant varieties of the NSP15 protein: S294A, S294T, Y343C, and Y343H. The structure of NSP15 S294A corresponds to a mutation of a key amino acid region with a neutral functional effect related to the replacement of Ser294 by Ala294 (replacement of a hydrophilic residue by a hydrophobic one at the ligand binding site) [21]. The S294T variety has an amino acid substitution of Ser293 for Thr293 (without changing

the functional effect); Y343C was obtained by replacing the amino acid residue Tyr343 with Cys 343, which is directly related to the ligand binding site; and the structure of Y343H corresponds to a mutation in the protein binding site with the replacement of Tyr343 by His343 [20].

Nonprotein components (water molecules, ions, cofactors, and ligands) were removed (DockThor), hydrogen atoms were added, and the hydrogen bond network was optimized taking into account pH 6.2 [22]. For mutant forms of NSP15, the wild type (with the PDB code: 6wxc) was used as the template. The proposed structures were used in this study; no additional correction of the protonation of amino acid residues was performed.

The experiments were carried out in the blind docking mode; the size of the approximating grating is 22 Å, the center is at X = 63.94, Y = –72.47, Z = 26.37, and the sampling step is 0.25 Å [17–20]. When analyzing the results, up to the five best configurations were taken into account.

Symmetric squarylium dyes were investigated: mono-, tri-, penta- and heptamethine cyanines, both cationic and anionic (having negatively charged sulfogroups), with various heterocycles (benzimidazolyl, benzothiazolyl, benzoxazolyl) and substituents in heterocycles. Trimethinecyanines (carbocyanines) also had various substituents in the heteroatoms and *meso*-position of the polymethine chain. To create PDB structures of ligand dyes and optimize their geometry (force field MMFF94), we used the Avogadro molecular editor [23]. For 3D visualization and analysis of the docking results, the UCSF Chimera program was used [24]. The original isomeric form of the *meso*-substituted carbocyanines corresponded to the *cis*-configuration as the most stable one for dyes of this type in polar solvents [25].

The stability of possible dye-protein complexes was judged by the sign and value of the total energy of the system E_{tot} obtained as a result of docking [17, 20]: it was assumed that the formation of stable complexes is more probable at sufficiently low (i.e., large in absolute value) negative energies.

RESULTS AND DISCUSSION

Molecular Docking of Cationic Carbocyanine and Neutral Squarylium Dyes with NSP15

The interaction of cationic *meso*-substituted carbocyanine (D1–D7) and neutral squarylium dyes (SD1–SD5) with various variants of NSP15 was studied. The structural formulas of the dyes are shown in Fig. 1. Carbocyanine dyes differ from each other as substituents in the *meso*-position of the polymethine chain, and by terminal hydrocycles. Squarylium dyes differ from each other by substituents R1 and R2.

The investigated cationic and neutral dyes are characterized by positive values of the total energy E_{tot} when interacting with all types of NSP15. In particular, when docking D1 and D7 with wild-type NSP15, we obtained $E_{tot} = 16.7 \pm 0.7$ and 55.4 ± 0.33 kcal mol^{-1}, respectively, which practically coincides with the result obtained for the mutant variant NSP15 Y343H. The smallest values of E_{tot} when docking with the wild type NSP15 were obtained for oxacarbocyanine D5 ($E_{tot} = 6.95 \pm 0.17$ kcal mol^{-1}) and for thiacarbocyanine D3 ($E_{tot} = 10.6 \pm 0.93$ kcal mol^{-1}). Note that for cationic carbocyanine dyes, the van der Waals energies (E_{vdW}) turned out to be negative: for dyes with different heterocycles, they are close to each other and range from -19.6 ± 3.32 kcal mol^{-1} (dye D4) to -27.8 ± 0.67 kcal mol^{-1} (dye D3). Similar results ($E_{tot} > 0$) were obtained earlier for cationic dyes during docking with the SARS-CoV-2 spike protein [16].

Positive E_{tot} values were obtained by docking uncharged squarylium dyes with NSP15. In particular, for dyes SD2 and SD3 with substituents R_1 = OH, values $E_{tot} = 59.4 \pm 1.15$ and 15.2 ± 0.79 kcal mol^{-1} (with the wild type NSP15), respectively. Docking with NSP15 unsubstituted SD1 gives a significantly more favorable (but also positive) energy value ($E_{tot} = 7.7 \pm 0.56$ kcal mol^{-1}). Similar data were obtained during the docking of neutral squarylium dyes with spike protein [16]. Positive E_{tot} values may indicate insufficient stability of complexes of cationic polymethine dyes and neutral squarilium dyes with NSP15.

Regardless of the use of mutant NSP15 subtypes, electrostatic energy, E_{el}, and van der Waals energy, E_{vdW}, turned out to be negative; for the majority of dyes, their average values were -13.7 ± 1.01 and -13.4 ± 3.7 kcal mol^{-1}, respectively. Bromosubstituted dyes SD4 and SD5 when docked with NSP15 (wild type) have $E_{vdW} = -29.1 \pm 0.62$ and -25.6 ± 0.26 kcal mol^{-1} and $E_{el} = -0.31 \pm 0.51$ and -1.28 ± 0.39 kcal mol^{-1}, respectively.

Molecular Docking of Anionic Dyes with NSP15

Anionic Squarylium Dyes. Together with uncharged (neutral) squarylium dyes (SD1–SD5), molecular docking of anionic squarylium dyes SD1.1–SD1.5 with NSP15 was carried out (the structures of the dyes are shown in Fig. 1). As a result of docking, negative values of the total energy ($E_{tot} < 0$) were obtained for most of the anionic squarylium dyes studied. In particular, upon the interaction of SD1.4 with the wild and mutant (Y343H) types of NSP15, $E_{tot} = -8.78 \pm 0.55$ and -9.46 ± 1.14 kcal mol^{-1}. At the same time, in the case of SD1.1, positive values $E_{tot} = 20.5 \pm 0.42$ and 20.6 ± 0.89 kcal mol^{-1} were obtained, respectively. This is possibly due to steric hindrances to the complex formation created by $C(CH_3)_3$ [16].

Strongly negative values E_{tot} were obtained by docking squarylium dyes SD1.2 and SD1.5; at the

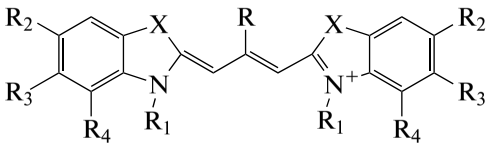

K1 –X = S, R = –CH_3, R_1 = –C_2H_5, $R_{2,3,4}$ = H

K2 –X = S, R = –OCH_3, R_1 = –C_2H_5, $R_{2,3,4}$ = H

K3 –X = S, R = –SCH_3, R_1 = –C_2H_5, $R_{2,3,4}$ = H

K4 –X = S, R = –Cl, R_1 = –C_2H_5, $R_{2,3,4}$ = H

K5 –X = O, R = –C_2H_5, R_1 = –CH_3, $R_{2,3,4}$ = H

K6 –X = O, R = –C_2H_5, R_1 = –C_2H, R_3 = –CH_3, $R_{2,4}$ = H

K7 –X = $C(CH_3)_2$, R = –CH_3, R_1 = –C_2H_5, $R_{2,3,4}$ = H

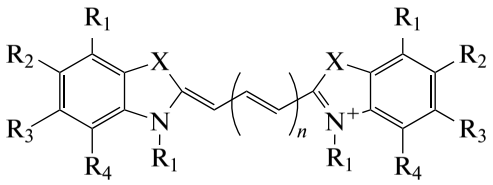

n = 0, R = –$(CH_2)_3SO_3^-$

1.1 –X = S, $R_{1–4}$ = H

1.2 –X = S, R_3 = –OCH_3, $R_{1,2,4}$ = H

1.3 –X = O, $R_{1–4}$ = H

1.4 –X = O, R_2 = –OCH_3, $R_{1,3,4}$ = H

1.5 –X = $C(CH_3)_2$, $R_{1–4}$ = H

n = 2, R = –$(CH_2)_3SO_3^-$

3.1 –X = S, R_{1-4} = H

3.2 –X = S, $R_{1,2,4}$ = H, R_3 = –OCH_3

3.3 –X = O, $R_{1,2,4}$ = H, R_3 = –OCH_3

3.4 –X = O, R_{1-4} = H

3.5 –X = S, $R_{1–4}$ = H, $R_{2,3}$ = –OCH_2O–

3.6 –X = $C(CH_3)_2$

3.7 –X = $C(CH_3)_2$, $R_{1,3,4}$ = H, R_2 = –SO_3^-

n = 3, R = –$(CH_2)_4SO_3^-$

4.1 –X = S, $R_{1–4}$ = H

4.2 –X = O, $R_{1–4}$ = H

4.3 –X = O, $R_{1,2,4}$ = H, R_3 = –OCH_3

4.4 –X = $C(CH_3)_2$, $R_{1,2}$ = –C_4H_4–, $R_{3,4}$ = H

n = 3, R = –$(CH_2)_3SO_3^-$

4.5 –X = $C(CH_3)_2$, $R_{1,3,4}$ = H, R_2 = –SO_3^-

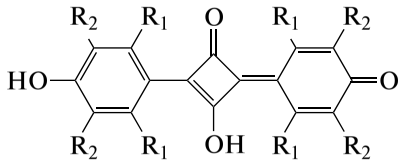

CK1 – $R_{1,2}$ = H

CK2 – R_1 = –OH, R_2 = H

CK3 – R_1 = –OH, R_2 = H

CK4 – R_1 = H, R_2 = Br

CK5 – R_1 = –OH, R_2 = Br

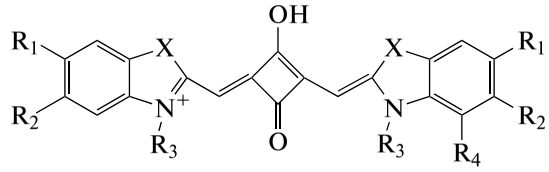

CK1.1 –X = $C(CH_3)_2$, R_1 = –SO_3^-, R_3 = –C_2H_5

CK1.2 –X = S, R_3 = –$(CH_2)_3SO_3^-$

CK1.3 –X = S, R_1 = –OCH_3, R_3 = –$(CH_2)_3SO_3^-$

CK1.4 –X = S, $R_{1,2}$ = –Cl, R_3 = –$(CH_2)_3SO_3^-$

CK1.5 –X = S, R_1 = –SO_3^-, R_3 = –C_2H_5

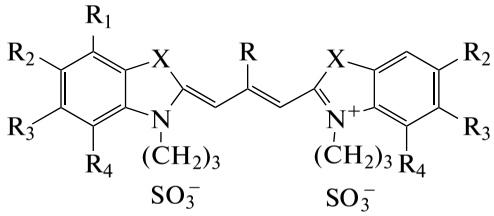

2.1 –X = S, R = –CH_3, $R_{1–4}$ = H

2.2 –X = S, R = –CH_3, $R_{1,2,4}$ = H, R_3 = –Cl

2.3 –X = O, R = –CH_3, $R_{1–4}$ = H

2.4 –X = O, R = –CH_3, $R_{1,2,4}$ = H, R_3 = –CH_3

2.5 –X = O, R = –CH_3, $R_{1,2}$ = H, $R_{3,4}$ = –C_4H_4–

2.6 –X = O, R = –C_2H_5, $R_{1,2,4}$ = H, R_3 = –CH_3

2.7 –X = O, R = –CH_3, $R_{1,2,4}$ = H, R_3 = –OCH_3

2.8 –X = $C(CH_3)_2$, R = –CH_3, $R_{1–4}$ = H

2.9 –X = $C(CH_3)_2$, $R_{1,3,4}$ = H, R_2 = –SO_3^-

Fig. 1. Structural formulas of cyanine dyes, as well as neutral and anionic squarylium dyes.

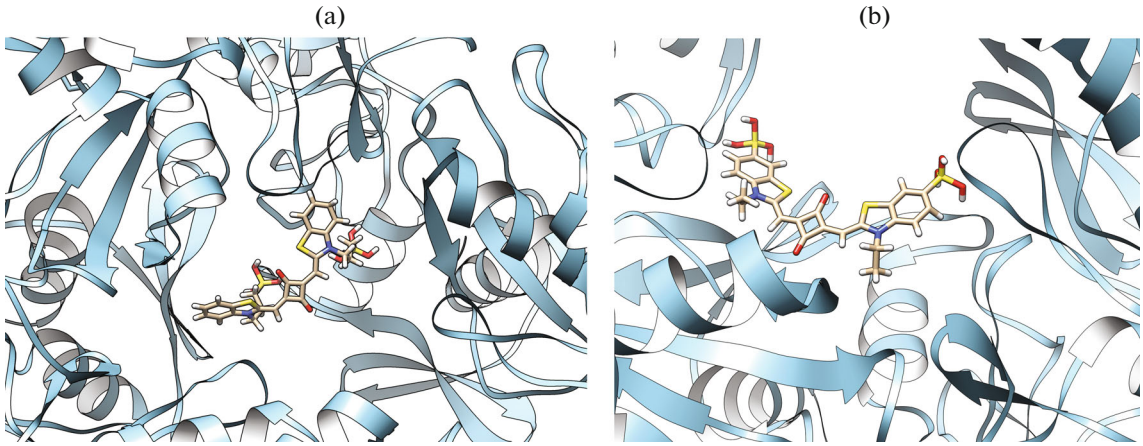

Fig. 2. Docking results with NSP15 dyes: (a) SD1.1 (wild type NSP15) and (b) SD1.5 (Y343H). The initial configurations of the dyes corresponded to *cis*-isomers.

same time, the most negative values of E_{tot} were obtained when docking with S294T for the dye SD1.2 ($E_{tot} = -72.1 \pm 1.32$ kcal mol^{-1}). The energies of electrostatic interaction and van der Waals for the anionic squarylium dyes SD1.1–SD1.5 turned out to be negative. The lowest values E_{el} (-57.2 ± 5.1 and -65.1 ± 3.4 kcal mol^{-1}, respectively) were obtained for dyes SD1.2 and SD1.4, which have sulfogroups in the substituents at N atoms. On average, for the studied anionic squarylium dyes, $E_{vdW} = -6.2 \pm 3.0$ kcal mol^{-1}, whereas $E_{el} = -55.7 \pm 8.5$ kcal mol^{-1}, i.e.; E_{el} is higher in absolute value than E_{vdW} by a factor of 4.2 to 20, which indicates a significant contribution of the forces of electrostatic interaction to the stabilization of the dye–protein complexes.

Squarylium dyes in complexes with NSP15 often take on a twisted (close to perplanar) configuration, for example, SD1.1. with the wild type NSP15 (Fig. 2a). However, the SD1.7 dye with all varieties of NSP15 is characterized by practically flat structures close to *trance*-isomers, in which the terminal heterocycles of the dye are only slightly (by ~20°) removed from the plane.

Docking places ligand molecules in the central cavity of the trimer near one of the protein subunits. Using the UCSF Chimera program [22], we analyzed the surface binding and searched for hydrogen bonds between the ligand and protein atoms, as well as for interatomic conflicts and contacts (based on the van der Waals radii of the molecules). The binding analysis showed that in a complex with NSP15, the squarylium dye molecules SD1.1 are located at a distance of ~4 Å from GLY165, and the TYR89 subunit C, the sulfogroup of the dye, is located at a distance of 4 Å from ARG91. In the cases of SD1.5 and mutant forms S294A and Y343H, docking gave almost identical positions of the ligands (interaction with subunit A). In the case of SD1.5 and Y343H (the structure of the dye in the complex is shown in Fig. 2b), the dye forms hydrogen bonds (2 Å) with GLN203 (with the participation of the terminal sulfogroup) and with ASP269 (due to the O atom of the squarylium ring). The search for interatomic contacts indicates the close (3 Å) contact of ARG92 with the sulfogroup of the dye; and the contact (4 Å) of GLU268 with the squarylium ring is also noted.

Anionic Cyanine Dyes. Molecular docking was also performed with a series of 26 anionic cyanines with different polymethine chain lengths: five anionic monomethinecyanine dyes (see Fig. 1, structures 1.1–1.5), nine *meso*-substituted trimethine cyanine dyes (carbocyanines, structures 2.1–2.9), seven pentamethine cyanine dyes (structures 3.1–3.7), and five heptamethine cyanine dyes (structures 4.1–4.5). The *meso*-substituted carbocyanines corresponded the *cis*-configurations.

Docking showed that ~90% of the selected compounds were characterized by negative values of the total energy ($E_{tot} < -19$ kcal mol^{-1}; see Table 1). Significant negative values E_{tot} were obtained for anionic monomethinecyanine dyes: for example, when docking dye 1.3, which is a benzoxazolyl derivative, with wild-type endoribonuclease, $E_{tot} = -83.8 \pm 1.8$ kcal mol^{-1}. Note that, for its analogs 1.1 and 1.5, we obtained ~30–44 kcal mol^{-1} E_{tot} value. It is possible that here, as in the case of the squarylium dyes, the steric factor plays a role, lowering E_{tot} (in absolute value) for the more bulky dyes 1.1 and 1.5 compared to 1.3.

The docking of carbocyanines (Fig. 1, structures 2.1–2.9) with NSP15 (wild type) also showed that these dyes can form energetically stable complexes. In particular, when docking oxacarbocyanines 2.3, 2.4, and 2.6, the values E_{tot} in the range -31.7 to -63.9 kcal mol^{-1} were obtained.

Table 1. Results of molecular docking of anionic cyanine dyes with NSP15 (wild type): total interaction energy of van der Waals energy and electrostatic interaction (kcal mol^{-1})

Dye	X	E_{tot}	E_{vdW}	E_{el}
1.1	S	−53.2 ± 0.86	−14.2 ± 3.34	−43 ± 4.12
1.2		−61.4 ± 0.66	−5.1 ± 7.7	−73.3 ± 7.05
1.3	O	−83.8 ± 1.81	0.25 ± 3.15	−73.8 ± 3.75
1.4		−76.2 ± 2.91	−0.96 ± 2.87	−74.6 ± 5.36
1.5	$C(CH_3)_2$	−39.8 ± 1.42	−5.9 ± 2.7	−50.3 ± 4.98
2.1	S	−49.6 ± 0.77	−4.4 ± 5.55	−83.3 ± 5.05
2.2		−51.7 ± 2.36	−1.5 ± 3.03	−83.7 ± 3.57
2.3	O	−57.9 ± 0.48	−4.2 ± 5.19	−67.3 ± 6.66
2.4		−55.1 ± 0.34	−11.1 ± 8.19	−62.7 ± 8.15
2.5		26 ± 1.07	−6.5 ± 4.71	−68.6 ± 3.97
2.6		−59.3 ± 0.42	−14.0 ± 1.06	−58.0 ± 3.15
2.7		36.9 ± 3.71	−3 ± 7.98	−71.7 ± 5.78
2.8	$C(CH_3)_2$	−36.4 ± 1.45	−7.6 ± 4.58	−53.8 ± 6.13
2.9	$C(CH_3)_2$	−96 ± 3.39	4.6 ± 4.93	−90.5 ± 6.97
3.1	S	2.7 ± 1.57	−8.1 ± 3.12	−58.3 ± 4.27
3.2		−55 ± 0.55	−3.9 ± 6.07	−67.7 ± 5.24
3.3	O	4.1 ± 2.01	−3.5 ± 6.51	−86.6 ± 7.85
3.4		−74.7 ± 2.32	−6.3 ± 10.93	−65.6 ± 11.8
3.5	S	−23.5 ± 1.04	−9.7 ± 6.02	−49.9 ± 5.39
3.6	$C(CH_3)_2$	−19.7 ± 0.69	−14.4 ± 6.82	−48.8 ± 2.6
3.7	$C(CH_3)_2$	−86.7 ± 0.28	4.3 ± 5.69	−87.6 ± 8.05
4.1	S	−43.4 ± 2.39	−9.8 ± 4.09	−61.9 ± 4.41
4.2	O	18.3 ± 1.01	−6.7 ± 6.22	−63.3 ± 6.03
4.3		−58.4 ± 0.88	−9.8 ± 4.56	−62 ± 4.51
4.4	$C(CH_3)_2$	8.9 ± 2.8	−11.2 ± 3.44	−58.1 ± 3.42
4.5	$C(CH_3)_2$	−77.8 ± 2.44	5.1 ± 3.31	−88.6 ± 5.54

Thiacarbocyanines 2.1 and 2.2 show comparable values of E_{tot} (see Table 1). Positive values E_{tot} were obtained for dyes 2.5 and 2.7 (Table 1), which have bulky substituents in heterocycles.

Negative E_{tot} values were obtained for most pentamethinecyanine (dicarbocyanine) dyes (in particular, for thiadicarbocyanine 3.2 and its oxa analog 3.4) with NSP15, which may indicate the stability of the intermolecular complexes of these dyes. For dyes 3.1 and 3.3, positive values were obtained for E_{tot} (2.7 ± 1.57 and 4.1 ± 2.01 kcal mol^{-1}, respectively). The values of the energies of electrostatic interaction and van der Waals for most pentamethine cyanine dyes (with the exception of 3.7) turned out to be negative; the smallest values of E_{el} (Table 1) were obtained for dyes 3.2 and 3.3 with $-OCH_3$ substituents. 1).

The study of the interaction of anionic heptamethinecyanine dyes (compounds 4.1–4.5) with NSP15 showed that noncovalent interaction is energetically possible for some of these dyes, leading to the formation of stable complexes ($E_{tot} < 0$). For dyes 4.2 (oxacyanin) and 4.4 (indoderivative), E_{tot} (18.3 ± 1.01 and 8.9 ± 2.8 kcal mol^{-1}, respectively) is positive.

The values E_{el} and E_{vdW} for most heptamethinecyanine dyes turned out to be negative, with the exception of dye 4.5 (for it, E_{vdW} = 5.1 ± 3.31 kcal mol^{-1}). For pentamethine cyanine (dicarbocyanine) dyes 3.1–3.6, the value E_{el} turned out to be 3.4–24 times higher

in absolute value than E_{vdW}; for heptamethine cyanine dyes 4.1–4.4, E_{el} was higher in absolute value than E_{vdW} by factors of 5.2 to 9.4. This indicates a significant contribution of the forces of electrostatic interaction to the stabilization of the dye–protein complexes. Indeed, molecular docking of indocarbocyanines with four sulfogroups (compounds 2.9, 3.7, and 4.5) gives significantly more negative values of the total energy (E_{tot} ~–77.8 to –96.0 kcal mol^{-1}) due to the large contribution of the electrostatic interaction to the stabilization of complexes (E_{el} ~–87.6 to –90.5 kcal mol^{-1}). The greatest negative values E_{tot} were obtained for indocarbocyanin 2.9 by docking with NSP15. Dyes with a longer polymethine chain show more moderate values of E_{tot} (see Table 1).

Docking of anionic cyanine dyes with mutant forms of the target protein (S294A, S294T, Y343C, and Y343H) showed almost the same binding energy parameters as for the wild type. For monomethinecyanine 1.1, the total energy values obtained for the four mutant forms practically coincide with the E_{tot} obtained for the original protein: -53.62 ± 0.49 and -53.2 ± 0.86 kcal mol^{-1}, respectively. A similar situation is observed in the case of other anionic dyes. Thus, for the pentamethine cyanine oxa dye 3.4, the values of E_{tot} obtained by docking with S294A, S294T, Y343C, and Y343H were -74.3 ± 1.56 kcal mol^{-1}; for the heptamethine oxa dye 4.2, docking with mutant forms gives $E_{tot} = -58.9 \pm 1.09$ kcal mol^{-1}, which, taking into account the confidence interval, corresponds to the data in Table 1. The only exception is the oxacarbocyanine dye 2.3, when docking with mutant forms of the protein for which E_{tot} decreases by 7% ($E_{tot} = -62.0 \pm 1.29$ kcal mol^{-1}).

Anionic cyanine dyes can bind to SARS-CoV-2 NSP15 in various conformations. Monomethine thiacyanines are characterized by a twisted (nonplanar) configuration of their molecules in the bound states; however, for oxa dyes 1.3 and 1.4, almost flat (energetically optimal) configurations are possible. For monomethinecyanine dyes, the analysis of surface binding did not reveal the presence of hydrogen bonds and interatomic conflicts.

Configurations close to planar are characteristic of carbocyanines 2.1, 2.2, and 2.3. In particular, for 2.2, docking with NSP15 (wild type) gives a dye configuration that is close to the *trance*-isomer configuration (Fig. 3a); in this case, the methyl group is almost perpendicular to the plane of one of the heterocycles, and the other heterocycle is rotated by an angle of ~15°. The interaction of oxacarbocyanin 2.3 and indocarbocyanin 2.8 is also characterized by an almost flat *trance*-configuration, while *meso*-substituents are displayed outside the planes. For dyes 2.4 and 2.6, the calculations give perplanar shapes twisted by ~45°. Docking of the 2.9 dye, which has an additional pair of sulfogroups, with NSP15 (wild type) suggests a distorted configuration close to a *trance*-isomer (Fig. 3d).

Docking pentamethinecyanines 3.1 and 3.2 with NSP15 gives strongly bent structures due to the distorted bond angles of the polymethine chain in which the terminal heterocycles are located almost parallel to each other. Dyes 3.4 (Fig. 3b) and 3.7 (they have 4 sulfogroups) acquire twisted (close to perplanar) structures upon interaction with NSP15; the dyes do not form hydrogen bonds and interatomic contacts with the protein.

For the docking of heptamethinecyanine dyes, various variants of molecular structures have been obtained, although mainly curved structures are characteristic of them. During the docking of dye 4.1, the distortions twist the terminal heterocyclic residues, and the substituents in positions 3 and 3' can be removed from the plane of the molecule (Fig. 3c). For dye 4.2, a structure with an almost perplanar position of terminal heterocycles was obtained; the dye does not form hydrogen bonds and interatomic contacts with NSP15. Dyes 4.3 and 4.5 (4 sulfogroups) have sickle-curved structures.

CONCLUSIONS

The results of molecular docking have shown that the noncovalent complexation of cyanine and squarylium dyes with SARS-CoV-2 NSP15 is significantly influenced by the Coulomb interactions in the dye–protein structure. Positive values of the total energy of the complex ($E_{tot} > 0$) for cationic cyanine (D1–D7) or neutral squarylium (SD1–SD5) dyes may indicate the instability of the complexes of these dyes with NSP15. For many anionic dyes, negative values of E_{tot} were obtained, which can characterize the higher stability of the corresponding complexes. Even more favorable results were obtained for indocarbocyanines with four sulfogroups that increase the negative charge of the dye molecule (2.9, 3.7, and 4.5). In addition, for most anionic dyes, the value E_{el} significantly exceeds in absolute value E_{vdW}, which also indicates the leading role of Coulomb forces in the formation of complexes. A similar effect of the Coulomb interaction on the stability of the dye–protein complex was found during the docking of cyanine dyes with the SARS-CoV-2 spike protein [16].

The structural differences in the dye molecules significantly affect the stability of the complexes. For oxa dyes, in general, more negative values were obtained for E_{tot} than for their analogs with thiazole and indole terminal heterocycles. Perhaps this is due to the more compact structure of oxa dyes than for the thia- and indo-analogs.

According to the E_{tot} value criterion characterizing the stability of complexes with NSP15, we can distinguish anionic squarylium dyes SD1.2 and SD1.5, monomethinecyanine anionic dyes 1.1–1.5, thia- and

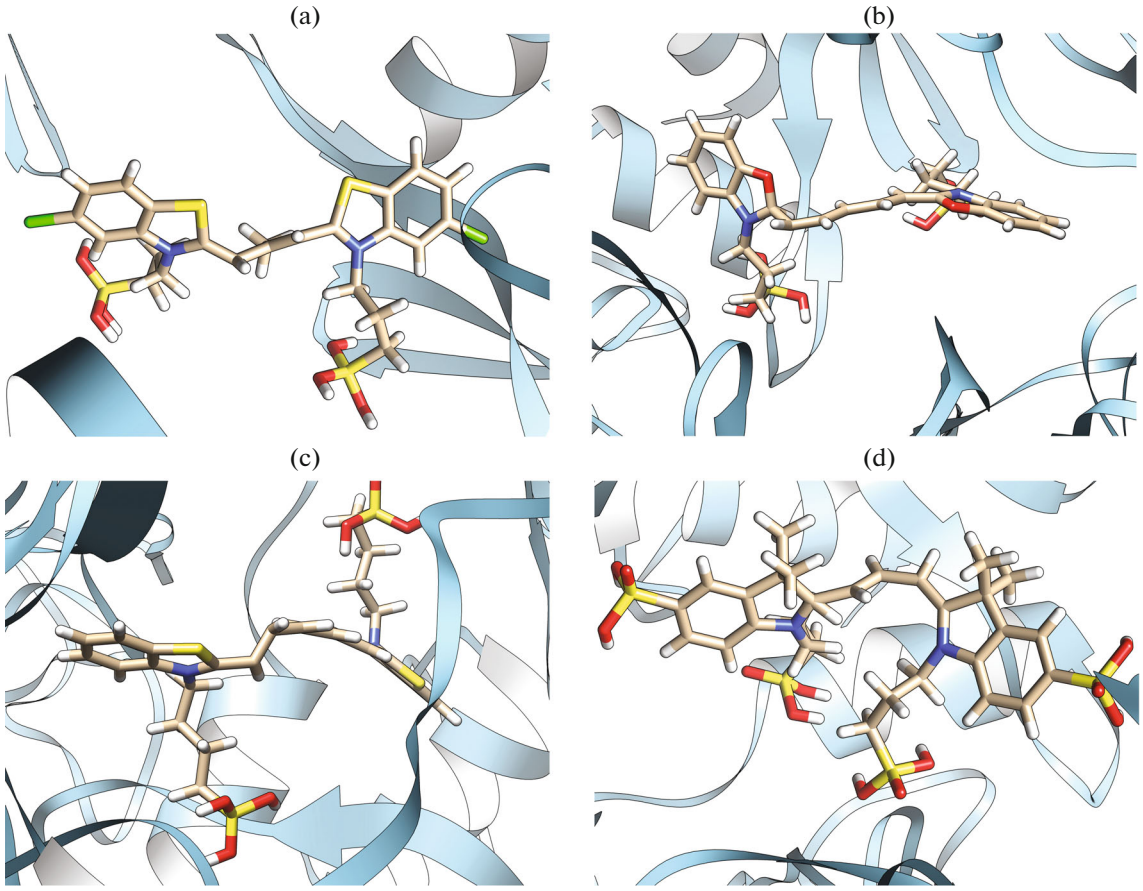

Fig. 3. Results of docking of anionic dyes with NSP15: 2.2 (a), 3.4 (b), 4.1 (c), and 2.9 (d).

oxa-cyanines 2.1–2.4, 2.6, 3.2, 3.4, 3.5, 4.1, and 4.3, indocyanines 2.8 and 3.6, as well as cyanines with four sulfogroups 2.9, 3.7, and 4.5.

When using dyes for the spectral detection of proteins, together with the stability of the dye–protein complexes, an important role is played by the change in the spectral-fluorescent properties of dyes during complexation. *Meso*-substituted carbocyanines (trimethinecyanines) are characterized by a sharper increase in the fluorescence intensity and more significant changes in the spectra due to the shift in the dynamic *cis-trance*-equilibrium, which makes it possible to detect very low concentrations of biomolecules when using dyes as fluorescent probes [7, 8, 10, 12, 26]. Considering the points made above, carbocyanines 2.1–2.4 and 2.6 are promising as such probes.

In complexes of carbocyanines with biomolecules, an intensification of the process of interconversion to the triplet state is observed, which leads to the population of the triplet energy levels [27–29]. This determines the possibility of photochemical reactions involving the excited triplet states of dyes in these systems and can potentially lead to the formation of reactive oxygen species (photodynamic effect). Thus, cyanines may be promising for light-induced damage to virus components (proteins to which the dye binds) and, thus, inactivation of the virus itself. Note that the UV photoinactivation of the MERS-CoV and SARS-CoV-2 coronaviruses in blood serum by riboflavin is currently being studied [30, 31]. From this point of view, *meso*-substituted thiacarbocyanines 2.1 and 2.2 can be isolated for further practical research in this area.

It should be noted that when docking cyanine dyes with mutant forms of NSP15—S294A, S294T, Y343C, and Y343H—the value E_{tot} practically coincided with that for the wild type NSP15 (there was a slight decrease in E_{tot} only for dye 2.3 when docking with mutant forms). This may indicate the efficacy of cyanine dye probes not only for the original form of the SARS-CoV-2 virus but also for its mutant forms, which is especially important now, when the mutant forms of SARS-CoV-2 are becoming more widespread in the world.

The molecular graphics and analyses performed with the UCSF Chimera software were developed by the University of California in San Francisco's Biocomputer, Imaging and Informatics Resource with support from NIH P41-GM103311.

FUNDING

The work was carried out within the framework of Russian Federation state assignment no. 001201253314 of the Institute of Biochemical Physics, Russian Academy of Sciences.

REFERENCES

1. V. K. Saarnio, K. Salorinne, V. P. Ruokolainen, et al., Dyes Pigm. **77**, 108282 (2020). https://doi.org/10.1016/j.dyepig.2020.108282
2. M. Eriksson, M. Hardelin, A. Larsson, J. Bergenholtz, and B. Akerman, J. Phys. Chem. B **111**, 1139 (2007). https://doi.org/10.1021/jp064322m
3. C. M. Soto, A. S. Blum, G. J. Vora, et al., J. Am. Chem. Soc. **128**, 5184 (2006). https://doi.org/10.1021/ja058574x
4. K. L. Robertson, C. M. Soto, M. J. Archer, O. Odoemene, and J. L. Liu, Bioconjugate Chem. **22**, 595 (2011). https://doi.org/10.1021/bc100365j
5. K. Vus, U. Tarabara, Z. Balklava, et al., J. Mol. Liq. **302**, 112569 (2020). https://doi.org/10.1016/j.molliq.2020.112569
6. G. S. Gopika, P. M. H. Prasad, A. G. Lekshmi, et al., Mater. Today: Proc. **46**, 3102 (2021). https://doi.org/10.1016/j.matpr.2021.02.622
7. A. S. Tatikolov, P. G. Pronkin, L. A. Shvedova, and I. G. Panova, Russ. J. Phys. Chem. B **13**, 900 (2019). https://doi.org/10.1134/S1990793119060290
8. A. V. Bychkova, P. G. Pronkin, O. N. Sorokina, A. S. Tatikolov, and M. A. Rosenfeld, Colloid. J. **76**, 387 (2014). https://doi.org/10.1134/S1061933X14040036
9. P. G. Pronkin and A. S. Tatikolov, High Energy Chem. **43**, 471 (2009). https://doi.org/10.1134/S0018143909060101
10. P. G. Pronkin and A. S. Tatikolov, J. Appl. Spectrosc. **82**, 438 (2015). https://doi.org/10.1007/s10812-015-0126-8
11. M. Yu. Anikovskii, A. S. Tatikolov, P. G. Pronkin, P. P. Levin, V. I. Sklyarenko, and V. A. Kuzmin, High Energy Chem. **37**, 398 (2003). https://doi.org/10.1023/B:HIEC.0000003399.44000.ec
12. P. G. Pronkin, L. A. Shvedova, and A. S. Tatikolov, Biophys. Chem. **261**, 106378 (2020). https://doi.org/10.1016/j.bpc.2020.106378
13. M. A. Beg and F. Athar, Pharm. Pharmacol. Int. J. **8**, 163 (2020). https://doi.org/10.15406/ppij.2020.08.00292
14. E. Tazikeh-Lemeski, S. Moradi, R. Raoufi, et al., J. Biomol. Struct. Dyn. **39**, 4633 (2021). https://doi.org/10.1080/07391102.2020.1779133
15. N. A. Al-Masoudi, R. S. Elias, and B. Saeed, Biointerface Res. Appl. Chem. **10**, 6444 (2020). https://doi.org/10.33263/BRIAC105.64446459
16. P. G. Pronkin and A. S. Tatikolov, Russ. J. Phys. Chem. B **15**, 25 (2021). https://doi.org/10.1134/S1990793121010267
17. I. A. Guedes, A. M. S. Barreto, D. Marinho, et al., Sci. Rep. **11**, 3198 (2021). https://doi.org/10.1038/s41598-021-82410-1
18. K. B. dos Santos, I. A. Guedes, A. L. M. Karl, and L. Dardenne, J. Chem. Inf. Model. **60**, 667 (2020). https://doi.org/10.1021/acs.jcim.9b00905
19. C. S. de Magalhaes, D. M. Almeida, H. J. C. Barbosa, and L. E. Dardenne, Inf. Sci. **289**, 206 (2014). https://doi.org/10.1016/j.ins.2014.08.002
20. I. A. Guedes, L. S. C. Costa, K. B. dos Santos, et al., Sci. Rep. **11**, 5543 (2021). https://doi.org/10.1038/s41598-021-84700-0
21. Y. Kim, R. Jedrzejczak, N. I. Maltseva, et al., Protein Sci. **29**, 1596 (2020). https://doi.org/10.1002/pro.3873
22. M. H. M. Olsson, C. R. Sondergaard, M. Rostkowski, and J. H. Jensen, J. Chem. Theory Comp. **7**, 525 (2011). https://doi.org/10.1021/ct100578z
23. M. D. Hanwell, D. E. Curtis, D. C. Lonie, et al., J. Cheminform. **4**, 1 (2012). https://doi.org/10.1186/1758-2946-4-17
24. Z. Yang, K. Lasker, D. Schneidman-Duhovny, et al., J. Struct. Biol. **179**, 269 (2012). https://doi.org/10.1016/j.jsb.2011.09.006
25. V. Khimenko, A. K. Chibisov, and H. Gorner, J. Phys. Chem. A **101**, 7304 (1997). https://doi.org/10.1021/jp971472b
26. P. G. Pronkin, L. A. Shvedova, and A. S. Tatikolov, J. Chem. Sci. **132**, 152 (2020). https://doi.org/10.1007/s12039-020-01858-2
27. P. G. Pronkin, A. S. Tatikolov, V. I. Sklyarenko, and V. A. Kuz'min, High Energy Chem. **40**, 252 (2003). https://doi.org/10.1134/S0018143906040096
28. P. G. Pronkin, A. S. Tatikolov, V. I. Sklyarenko, and V. A. Kuz'min, High Energy Chem. **40**, 403 (2006). https://doi.org/10.1134/S0018143906060087
29. A. S. Tatikolov, Russ. J. Phys. Chem. B **15**, 33 (2021). https://doi.org/10.1134/S1990793121010280
30. S. D. Keil, R. Bowen, and S. Marschner, Transfusion **56**, 2948 (2016). https://doi.org/10.1111/trf.13860
31. S. D. Keil, I. Ragan, S. Yonemura, et al., Vox Sang **115**, 495 (2020). https://doi.org/10.1111/vox.12937